Graphene Actuators

DOI: 10.1002/ange.201304358

Graphene Fibers with Predetermined Deformation as Moisture-Triggered Actuators and Robots**

*Huhu Cheng, Jia Liu, Yang Zhao, Chuangang Hu, Zhipan Zhang, Nan Chen, Lan Jiang, and Liangti Qu**

Smart materials and structures with fast, reversible, controllable shape changes in response to environmental stimuli have attracted tremendous attention due to their remarkable potential in applications ranging from robots and sensors to memory chips.[1] Although it poses a considerable challenge, responsive behavior, especially in a predefined fashion, has become a key function for advanced artificial actuating and shape-memory structures and devices.[2] Graphene-based structures exhibit many exciting properties[3] that could benefit such actuation systems.[4] In this context, we have constructed electrochemical actuators based on unimorph and bilayer graphene films, and three-dimensional graphene skeletons.[5] However, most of these aforementioned actuators are based on simple displacement or deformation, and do not display sophisticated motion and precise shape control in a predefined manner.

Recently, we, along with other groups,[6] have successfully fabricated graphene fibers (GFs) by directly assembling graphene oxide (GO) through a dimension-confined hydrothermal strategy and a large-scale spinning method. These new types of fibers possess the common characteristics of fibrillar materials like the mechanical flexibility required for textiles, yet are unique in that they are lightweight and easy to functionalize in comparison to conventional carbon fibers. These remarkable features endow them with prominent advantages for the development of unconventional, flexible, stimulus-responsive structures, especially in fiber form, for weavable intelligent devices. To the best of our knowledge, however, smart actuators based on GFs have not been reported.

[*] H. Cheng, J. Liu, Y. Zhao, C. Hu, Dr. Z. Zhang, Dr. N. Chen, Prof. L. Qu
Key Laboratory of Cluster Science, Ministry of Education
School of Chemistry, Beijing Institute of Technology
Beijing Key Laboratory of Photoelectric/Electrophotonic Conversion Materials
Beijing 100081 (China)
E-mail: lqu@bit.edu.cn
Homepage: http://sc.bit.edu.cn/kyjgjktz/qltktz/index.htm
Prof. L. Jiang
Laser Micro-/Nano-Fabrication Laboratory, Beijing Institute of Technology (China)

[**] This work was supported financially by the National Basic Research Program of China (2011CB013000) and NSFC (21004006, 21174019).

Supporting information for this article (including experimental details) is available on the WWW under http://dx.doi.org/10.1002/anie.201304358.

Herein we describe the rational design and fabrication of graphene/graphene oxide (G/GO) fibers which are region-asymmetric as a result of the positioned laser reduction of freshly spun GO fibers. Remarkably, the G/GO fibers display complex, well-confined, predetermined motion and deformation once exposed to moisture. Apart from their application as a single-fiber walking robot, shape-memory G/GO fibers will play a vital role for the construction of the woven devices and smart textiles as we shall see later.

The laser-assisted reduction of GO has been demonstrated to be a facile and efficient approach for the region-specific conversion of GO into G[7] and provides an opportunity for the region-selective reduction of GO fibers in a well-controlled manner. As shown in Figure 1a, an asymmetric G/GO fiber can be conveniently fabricated by scanning a laser beam along a preformed GO fiber such that the scanned area is converted to G (also called reduced GO) and the unexposed region remains unchanged. During the laser scanning, the color change from yellow-brown for GO to black for the scanned surface on the GO fiber was observed clearly (Figure 1b). Meanwhile, distinctive features also appear in the scanning electron microscopy (SEM) image (Figure 1c). The laser-reduced region looks normal under electron irradiation, suggesting that the reduced GO is electrically conductive, but the scanned and unscanned regions have similar surface morphologies (Figure S1).

To roughly estimate the conductivity, we investigated the current–voltage (I–V) curves of the surfaces of a laser-reduced GO fiber and the initial GO fiber (Figure 1d). The plot for the laser-treated fiber has a significantly higher slope than that for the GO fiber, which leads to a conductivity of roughly $2\times10^{8}\,\Omega\,m^{-1}$ for the G surface, nearly two orders of magnitude greater than that of the GO surface (ca. $5\times10^{10}\,\Omega\,m^{-1}$).

Figure 1e,f show the typical side view of the initial GO fiber and the asymmetric G/GO fiber, respectively. The black boundary (G region) along the G/GO fiber is clearly observed (Figure 1f), while it is absent for the GO fiber (Figure 1e). The laser-induced G region makes up approximately one-third of the surface area of the fiber with a reduction depth of about 15–20 μm, which is predetermined by the laser control system (see the Supporting Information). The asymmetry of the G/GO fiber is also evident in SEM images (Figure S2).

The bright parts in Figure 1c,e,f for the GO surfaces have obvious high O content with an O/C atomic ratio of approximately 1:3 as verified by energy-dispersive X-ray spectra (EDS; Figure 1g). However, the laser-induced G regions have a much lower O level (O/C ≈ 1:8), indicating a high degree of GO reduction by the laser irradiation.

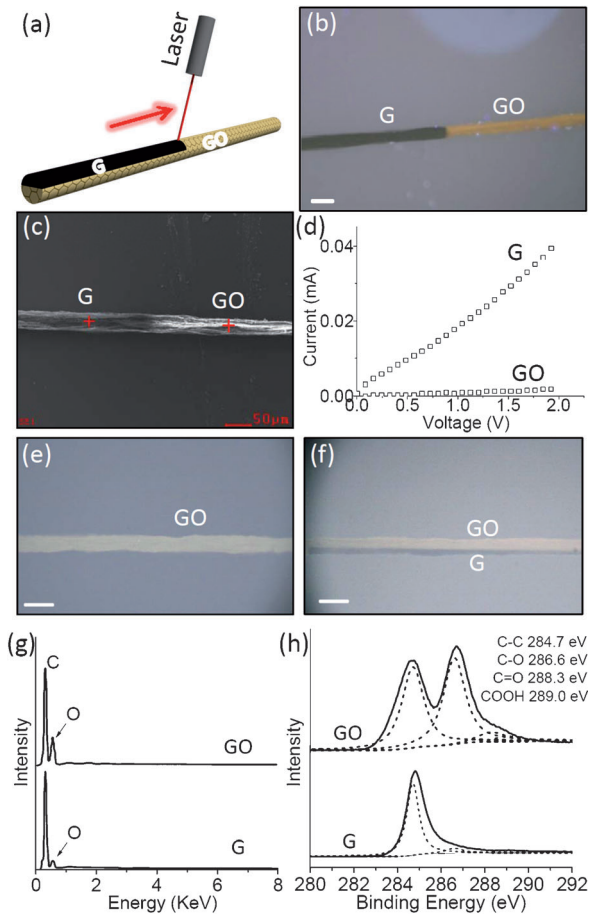

Figure 1. a) Representation of positioned laser reduction on one side of a GO fiber. The black region corresponds to the laser-induced G region along the brown GO fiber. Photomicrograph (b) and SEM image (c) of the top surface of the as-prepared asymmetric G/GO fiber. d) *I–V* curves for a laser-induced G fiber and an untreated GO fiber with a length of 1 cm. e,f) Photographs (side view) of the initial GO fiber and the asymmetric G/GO fiber, respectively. g) EDS analysis of the initial GO fiber and the laser-induced G region. h) C1s XPS peaks of initial GO and laser-induced G recorded with a thin film. Scale bars: 50 µm.

Raman spectra also indicate that the GO fiber was reduced and its conjugated structures were partly restored (Figure S3). To further confirm the effectiveness of the laser reduction of GO, we also carried out X-ray photoelectron spectroscopy (XPS) analysis on a GO thin film scanned with a laser under conditions similar to those applied for the reduction on the GO fiber. We found that in the laser-induced G region the oxygen-containing groups had been removed significantly compared to the initial GO (Figure 1h and Figure S4). The C1s spectrum of the original GO (Figure 1h) reveals four types of carbon-containing bonds: C=C/C–C (284.7 eV), C–O (hydroxy and epoxy groups, 286.6 eV), C=O (carbonyl, 288.3 eV), and O–C=O (carboxyl, 289 eV). For the laser-induced G sample, however, the C–C bonds become dominant (Figure 1h); the O/C atomic ratio is roughly 1:9, which is similar to the previously mentioned EDS result and again verifies the efficient reduction of GO by laser irradiation. In good agreement with the XPS results, X-ray diffraction (XRD) patterns confirm that the typical diffraction peak of GO at approximately 11° has completely disappeared for the laser-induced G (Figure S5).

The G/GO fibers are flexible enough for arbitrary deformation (Figure S6) and have a high tensile strength of up to 100 MPa, similar to that of pure GO fibers (Figure S7), which will benefit the applications in fiber and textile devices. Due to the oxygen-rich functional groups of GO and the unique stacking of GO sheets, water has a stronger affinity with the GO layers than with the G structure, and the relatively fast and reversible expansion/contraction of GO layers is evidenced through the adsorption and desorption of water vapor.[8] Therefore, the asymmetric G/GO fiber developed in this study should behave as a moisture-sensitive fiber actuator (Figure 2a).

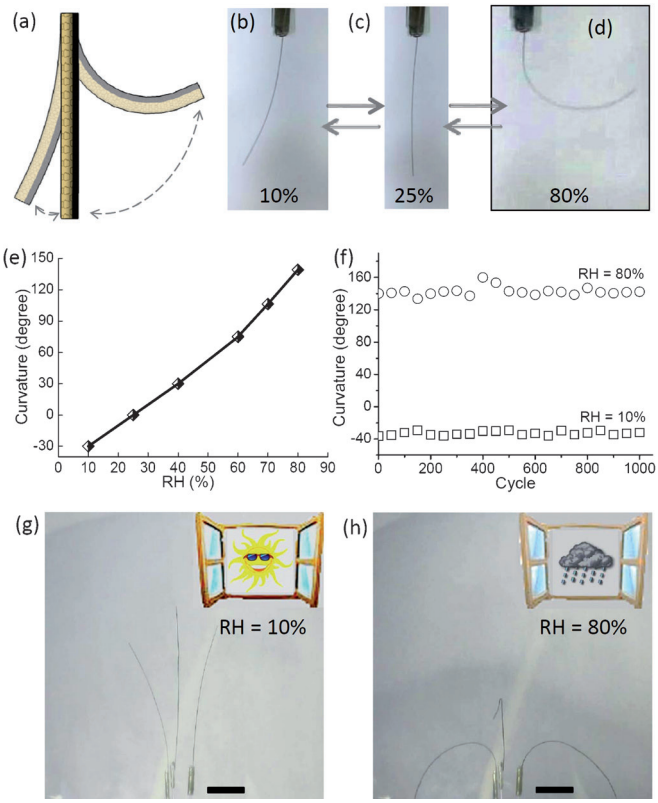

Figure 2. a) Representation of the possible bending of a G/GO fiber exposed to different relative humidities. b–d) Photographs of a G/GO fiber (2 cm in length) under different relative humidities. e) Plot of the curvature of a G/GO fiber versus RH. f) Durability test for a G/GO fiber undergoing repeated changes in relative humidity. g,h) Photographs of three-wire moisture tentacles made of the G/GO fibers on a sunny and a rainy day, respectively; scale bars: 5 mm.

As expected, a rapid bending to the G side occurs once the G/GO fiber (Figure 2c) is exposed to moist air with a relative humidity (RH) of 80% (Figure 2d), while the fiber recovers to the initial state when it returned to the ambient conditions (Figure 2c and Movie S1). This process is fully reversible with an average motion rate of approximately $8°s^{-1}$, indicating the reliable shape-memory feature of the G/GO fiber. Since the

G/GO fiber was obtained by laser reduction of a GO fiber under lab conditions (RH = 25%), a decrease in the RH will lead to the deformation of the G/GO fiber to the GO side (Figure 2b) due to the contraction of GO layers caused by loss of adsorbed water.

The bending degree of the G/GO fiber is reflected by the mean angle of curvature (θ) and the θ change in response to different RH is presented in Figure 2e. As can be seen, the as-prepared G/GO fiber rapidly bends from 0° to 140° when the RH increases from 25% to 80%. When the RH is less than that under ambient conditions (RH = 25%), the G/GO fiber gradually moves in the opposite direction with a bending angle of roughly −30° at RH = 10%. The deformation of the G/GO fiber towards the G side at RH = 25% is more facile than that towards the GO side at RH = 25%, probably because of the tensile strength from the moisture-insensitive G layers. It was found that the increased reduction of GO could lead to improved actuation response (Figure S8). After 1000 cycles of repeated humidity alteration between 10% and 80%, the response performance remained stable (Figure 2f). Good durability has also been observed for G/GO fiber at different relative humidities (Figure S9). These results validate the highly reliable actuation behavior of the G/GO fiber.

Making use of the sensitive response of the G/GO fibers, we further designed the three-wire moisture tentacles. As shown in Figure 2g,h, the tentacles stand gracefully in a sunny day, while they lower their heads when rain is coming. The G/GO fibers are available for the construction of various devices with specific applications such as the moisture-triggered claw in Figure S10 and Movie S2.

We also designed region-specifically asymmetric G/GO fibers for use as complex deformation-predefined actuators. As shown in Figure 1a, the reduction of GO occurs on the GO fiber in a well-controlled "spot reduction" upon laser irradiation. We generated a 0.5–1 mm long G region along the GO fiber (Figure 3a,b; see Figure S11). In this case, the moisture-insensitive G region deforms like a hinge to allow the reversible folding of the fiber at this point due to the expansion/contraction of the GO fiber in response to the humidity variation (Figure 3c). Indeed, a folded structure appears (Figure 3e) when the regionally reduced GO fiber is exposed to moisture (RH = 80%); the fiber subsequently recovers to its initial state after the applied moisture bias is removed.

By rational design and localization of the laser-induced G regions along the GO fiber, more sophisticated shape changes can be achieved. As exemplified in Figure 3f–i, three G regions were positioned on the two sides of GO fiber (Figure 3f), which will lead to three kinks in the GO fiber upon exposure to moisture (Figure 3g). The spontaneously formed "hook" is validated experimentally in Figure 3h,i.

The programmable, positioned reduction of GO fibera by laser scanning is indeed powerful for the manufacture of tailored fiber actuators. As shown in Figure 3j–m, alternating, asymmetric G/GO segments along the fiber will produce "S"-shaped actuation. More interestingly, a G/GO fiber with a spiral reduction pattern initially lying on glass slide was rapidly transformed into a self-supporting spring structure at RH = 80% (Figure 3n–q, Figure S12, and Movie S3).

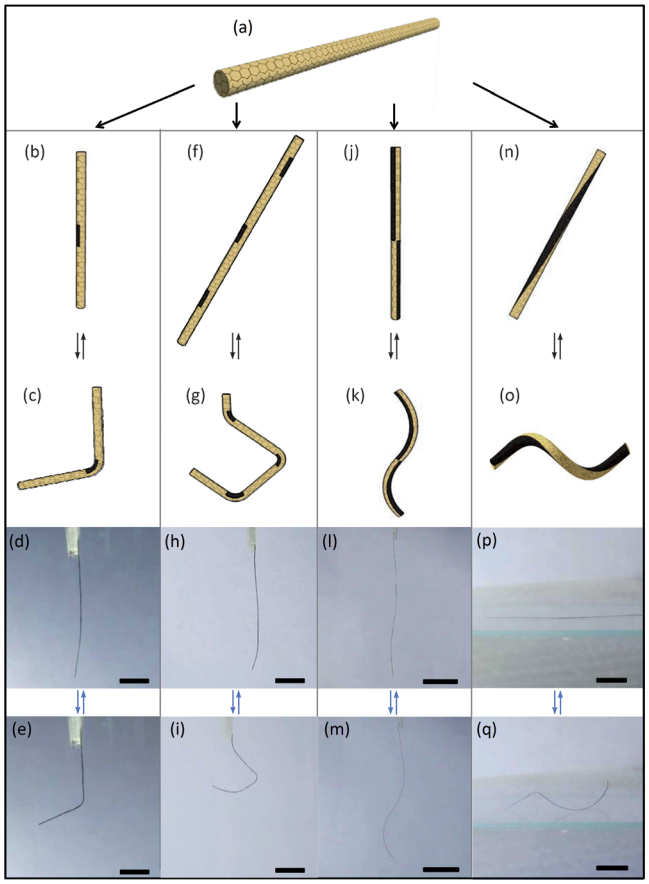

Figure 3. Schematic diagrams and photographs of different designed G/GO fibers and their reversible deformations with changes in humidity. a) The initial GO fiber. b,f,j,n) GO fibers with region-confined laser reduction. In (b) and (f) the length of reduced regions is about 1 mm, in (j) it is about 2 cm. c,g,k,o) The corresponding predefined deformations upon exposure of the fibers in (b,f,j,n) to moisture. d,h,l,p) Photographs of GO fibers corresponding to the states in (b,f,j,n). e,i,m,q) Deformations of the fibers in (d,h,l,p) at RH = 80%. Scale bars: in (d,e,p,q): 5 mm; in (h,l,m): 1 cm.

The structure-defined deformation provides the opportunity for the versatile manipulation of G/GO fibers. An example included in Figure S13 is the reversible transformation of parallel lines of predesigned G/GO fibers to form the letters "OK" in response to a change in relative humidity. The pliability of G/GO fibers also facilitates weaving them into a self-supported, stable textile structure (Figure 4a), which bends when exposed to moisture while maintaining the fiber network (Figure 4a). When the moisture is removed, the bent textile recovers its shape almost completely (Figure 4b). These results indicate the great potential applications of G/GO fibers in stimulus-responsive textiles.

The excellent humidity-responsive bending/unbending ability of the G/GO fibers enabled us to build a new type of microfiber walking devices. Unlike the conventional film-based walking devices that move along open spaces,[9] the G/GO fiber walker can travel in a narrow slit. As shown in Figure 4c, we put the G/GO fiber walker between two glass slides with a gap of roughly 1 mm, which is also supported by a ratchet substrate (Figure S14) like that used with other

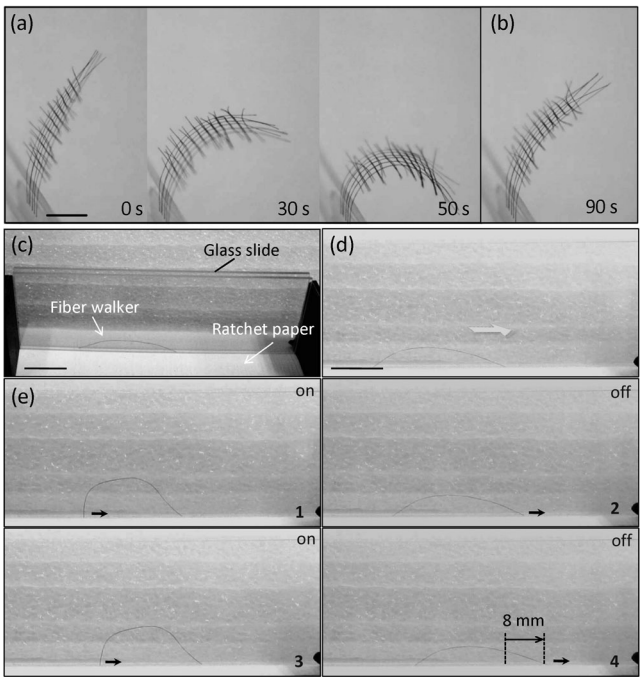

Figure 4. Responsive textile and walking robot. a) Photographs of a hand-woven textile-like network of G/GO fibers exposed to RH = 80% at different exposure times, and b) a photograph of the same fiber after moisture has been removed. The textile is composed of short GO fibers and long G/GO fibers with the G sides at the front of the network. c) Photograph of the G/GO fiber walker within the narrow slit between two glass slides on the ratchet paper. d) The initial state of the G/GO fiber walker, which is manually bent a little in advance to have a standing pose. e) A series of photographs of the G/GO fiber walker crawling on the ratchet paper in response to the "on" and "off" states of applied moisture. The G side of G/GO fiber is placed downwards. RH("on" state) = 80%, RH("off" state) = 25%. Scale bars in (a,b): 5 mm; in (c,d) = 1 cm.

walkers.[9,10] Initially, the G/GO fiber walker stands there under ambient conditions (Figure 4d). Once the relative humidity increases, its back end shifts due to the increased bending (Figure 4e, stage 1). During the stretching process induced by the removal of moisture, the front end of the G/GO fiber walker slides forward while the back tip is fixed by the indentations on the rough surface of the substrate (Figure 4e, stage 2). With the alternation of the relative humidity, the device walks unidirectionally step by step with a moving rate of 4 mm per cycle (Figure 4e, stages 1–4, and Movie S4) despite the absence of systematical device optimization. In principle, the moving speed and motion of this proof-of-concept prototype for the walking robot could be readily improved by regulating the frequency of the humidity alternation and also the device length. It should also be noted that the walking G/GO fiber may also work in open space since it can deform to a self-supported structure during humidity alteration (Figure 3o,q).

To understand the deformation of the G/GO fiber, we quantitatively investigated the changes in the length of the GO fiber and its laser-reduced counterpart. As shown in Figure 5, the GO fiber displayed a fast (about 10 s) and rhythmic length change by roughly 5% in response to the

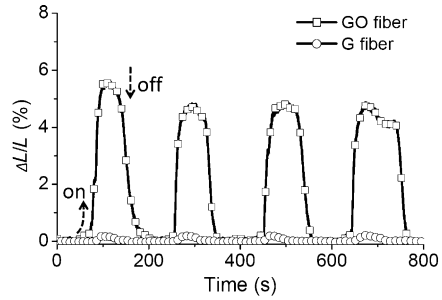

Figure 5. The length changes of the GO fiber and laser-induced G fiber in response to the alternation between RH = 25% and RH = 80% (L and ΔL are defined as the length and length change of the fibers).

humidity changes, while the G fiber exhibited a negligible strain fluctuation (ca. 0.25%). The length change for the GO fiber is 20 times that of its laser-treated counterpart, indicating the deformation of G/GO fiber is mainly determined by the shape change of GO. On the basis of the double-layer model (Figure S15), the curvature (θ) of the G/GO fiber is roughly estimated to be up to about 2000° at RH = 80% without considering possible influences such as the interaction of the bilayers and their inherent mechanical rigidity, the columnar structure of the G/GO fiber, and the change in diameter with applied humidity (Figure S16). Preliminary experimental data show that a 2 cm long G/GO fiber can bend roughly 140° (Figure 2), implying that there is considerable room to further enhance the actuator performance through the structural optimization.

In conclusion, the asymmetric G/GO fiber structures obtained by positioned laser reduction of GO fibers display complex, well-controlled motion and deformation in a predetermined manner once exposed to moisture. This work not only offers a strategy for producing region-asymmetric G/GO fibers, but also demonstrates that they can be deformed deliberately and can walk as a single-fiber robot along a channel. The unique G/GO fibers provide a new platform for the development of the woven devices and smart textiles beyond those demonstrated in this preliminary study.

Received: May 21, 2013
Published online: August 14, 2013

Keywords: actuators · carbon · graphene fibers · laser reduction · mechanical properties

[1] a) P. Kim, C. M. Lieber, *Science* **1999**, *286*, 2148–2150; b) S. V. Ahir, E. M. Terentjev, *Nat. Mater.* **2005**, *4*, 491–495; c) A. M. Fennimore, T. D. Yuzvinsky, W. Q. Han, M. S. Fuhrer, J. Cumings, A. Zettl, *Nature* **2003**, *424*, 408–410; d) J. E. Jang, S. N. Cha, Y. J. Choi, S. J. Kang, T. P. Butler, D. G. Hasko, J. E. Jung, J. M. Kim, G. A. J. Amaratunga, *Nat. Nanotechnol.* **2008**, *3*, 26–30.

[2] a) A. Sidorenko, T. Krupenkin, A. Taylor, P. Fratzl, J. Aizenberg, *Science* **2007**, *315*, 487–490; b) M. M. Ma, L. Guo, D. G. Anderson, R. Langer, *Science* **2013**, *339*, 186–189.

[3] a) A. K. Geim, *Science* **2009**, *324*, 1530–1534; b) S. Stankovich, D. A. Dikin, G. H. B. Dommett, K. M. Kohlhaas, E. J. Zimney, E. A. Stach, R. D. Piner, S. B. T. Nguyen, R. S. Ruoff, *Nature*

2006, *442*, 282 – 286; c) G. Eda, G. Fanchini, M. Chhowalla, *Nat. Nanotechnol.* **2008**, *3*, 270 – 274; d) P. Blake, P. D. Brimicombe, R. R. Nair, T. J. Booth, F. Schedin, L. A. Ponomarenko, S. V. Morozov, H. F. Gleeson, E. W. Hill, A. K. Geim, *Nano Lett.* **2008**, *8*, 1704 – 1708; e) Y. Q. Sun, Q. Wu, G. Q. Shi, *Energy Environ. Sci.* **2011**, *4*, 1113 – 1132.

[4] a) Y. Huang, J. J. Liang, Y. S. Chen, *J. Mater. Chem.* **2012**, *22*, 3671 – 3679; b) C. H. Zhu, Y. Lu, J. Peng, J. F. Chen, S. H. Yu, *Adv. Funct. Mater.* **2012**, *22*, 4017 – 4022; c) C. Z. Wu, J. Feng, L. L. Peng, Y. Ni, H. Y. Liang, L. H. He, Y. Xie, *J. Mater. Chem.* **2011**, *21*, 18584 – 18591; d) J. Zhang, F. Zhao, Z. P. Zhang, N. Chen, L. T. Qu, *Nanoscale* **2013**, *5*, 3112 – 3126; e) L. H. Lu, J. H. Liu, Y. Hu, Y. W. Zhang, W. Chen, *Adv. Mater.* **2013**, *25*, 1270 – 1274; f) J. J. Liang, L. Huang, N. Li, Y. Huang, Y. P. Wu, S. L. Fang, J. Y. Oh, M. Kozlov, Y. F. Ma, F. F. Li, R. Baughman, Y. S. Chen, *ACS Nano* **2012**, *6*, 4508 – 4509.

[5] a) X. J. Xie, L. T. Qu, C. Zhou, Y. Li, J. Zhu, H. Bai, G. Q. Shi, L. M. Dai, *ACS Nano* **2010**, *4*, 6050 – 6054; b) X. J. Xie, H. Bai, G. Q. Shi, L. T. Qu, *J. Mater. Chem.* **2011**, *21*, 2057 – 2059; c) J. Liu, Z. Wang, X. J. Xie, H. H. Cheng, Y. Zhao, L. T. Qu, *J. Mater. Chem.* **2012**, *22*, 4015 – 4020; d) J. Liu, Z. Wang, Y. Zhao, H. H. Cheng, C. G. Hu, L. Jiang, L. T. Qu, *Nanoscale* **2012**, *4*, 7563 – 7568.

[6] a) Z. Xu, C. Gao, *Nat. Commun.* **2011**, *2*, 571; b) Z. L. Dong, C. C. Jiang, H. H. Cheng, Y. Zhao, G. Q. Shi, L. Jiang, L. T. Qu, *Adv. Mater.* **2012**, *24*, 1856 – 1861; c) H. P. Cong, X. C. Ren, P. Wang, S. H. Yu, *Sci. Rep.* **2012**, *2*, 613; d) C. G. Hu, Y. Zhao, H. H. Cheng, Y. Wang, Z. L. Dong, C. C. Jiang, X. Q. Zhai, L. Jiang, L. T. Qu, *Nano Lett.* **2012**, *12*, 5879 – 5884; e) Y. Zhao, C. C. Jiang, C. G. Hu, Z. L. Dong, J. L. Xue, Y. N. Meng, N. Zheng, P. W. Chen, L. T. Qu, *ACS Nano* **2013**, *7*, 2406 – 2412.

[7] a) W. Gao, N. Singh, L. Song, Z. Liu, A. L. M. Reddy, L. J. Ci, R. Vajtai, Q. Zhang, B. Q. Wei, P. M. Ajayan, *Nat. Nanotechnol.* **2011**, *6*, 496 – 500; b) Y. L. Zhang, L. Guo, S. Wei, Y. Y. He, H. Xia, Q. D. Chen, H. B. Sun, F. S. Xiao, *Nano Today* **2010**, *5*, 15 – 20; c) M. F. El-Kady, V. Strong, S. Dubin, R. B. Kaner, *Science* **2012**, *335*, 1326 – 1330.

[8] a) R. R. Nair, H. A. Wu, P. N. Jayaram, I. V. Grigorieva, A. K. Geim, *Science* **2012**, *335*, 442 – 444; b) Z. Jian, M. A. Christine, D. X. Jia, R. Ayyalusamy, T. Thomas, A. K. Nicholas, *ACS Nano* **2012**, *6*, 8357 – 8365; c) P. Sungjin, J. An, J. W. Suk, R. S. Ruoff, *Small* **2010**, *6*, 210 – 212.

[9] Y. Ma, Y. Y. Zhang, B. S. Wu, W. P. Sun, Z. G. Li, J. Q. Sun, *Angew. Chem.* **2011**, *123*, 6378 – 6381; *Angew. Chem. Int. Ed.* **2011**, *50*, 6254 – 6257.

[10] a) S. Maeda, Y. Hara, T. Sakai, R. Yoshida, S. Hashimoto, *Adv. Mater.* **2007**, *19*, 3480 – 3484; b) M. Moua, R. R. Kohlmeyer, J. Chen, *Angew. Chem. Int. Ed.* **2013**, DOI: 10.1002/anie.201210232.